Article | Received 21 July 2025; Revised 8 September 2025; Accepted 17 September 2025; Published 23 September 2025
https://doi.org/10.55092/sc20250025

A comparative analysis of explainable artificial intelligence (XAI) models for predicting concrete elastic dynamic modulus

Haoyang Zheng[1], Yuxiang Huang[1], Kechang Wu[1], Bowen Wang[1], Qingyuan Hu[1], Dianchao Wang[2], Bochao Sun[1,*] and Maxwell Fordjour Antwi-Afari[3,*]

[1] College of Civil Engineering and Architecture, Zhejiang University, Hangzhou, China
[2] Department of Architecture, Graduate School of Engineering, The University of Tokyo, Tokyo, Japan
[3] Department of Civil Engineering, College of Engineering and Physical Sciences, Aston University, Birmingham B4 7ET, UK

* Correspondence authors; E-mails: sunbochao@zju.edu.cn (B.S.); m.antwiafari@aston.ac.uk (M.F.A.).

Highlights:

- Compared five XAI methods for predicting concrete elastic modulus under freeze–thaw cycles.
- GAMI-Net showed the highest accuracy and strongest interpretability.
- Freeze–thaw cycles and water content were identified as key factors in degradation.
- Heatmaps from GAMI-Net/EBM offered clearer interaction insights than SHAP.
- GAMI-Net is proposed as a reliable tool for designing frost-resistant concrete.

Abstract: The application of explainable artificial intelligence (XAI) in civil engineering has garnered increasing attention due to its ability to enhance transparency in machine learning (ML) models for material behavior prediction. However, the comparative performance and interpretability of various XAI models in predicting concrete properties under freeze–thaw degradation remain underexplored. This study presents a comprehensive evaluation of five XAI approaches: GAMI-Net, Explainable Boosting Machine (EBM), SHapley Additive exPlanations (SHAP), Local Interpretable Model-agnostic Explanations (LIME), and Shapash, for predicting the elastic dynamic modulus of concrete subjected to freeze–thaw cycles. Using a dataset comprising 347 concrete test records, three predictive models (GAMI-Net, EBM, and XGBoost) were developed, with post-hoc explanations applied to XGBoost outputs. Model performance was assessed through accuracy metrics and interpretability analyses, including feature importance ranking, global and local explanation visualizations, and dependence plots. The results reveal that GAMI-Net achieved the best overall performance (RMSE = 0.04, R^2 = 0.95) and provided the most stable and physically consistent interpretations. Freeze–thaw cycles and water content were identified as the most critical factors, with their interaction accounting for the greatest influence on concrete degradation. Two-dimensional heatmaps from GAMI-Net and EBM offered more intuitive interaction insights compared to SHAP-based visualizations. This study contributes theoretically by validating the efficacy of inherently interpretable models for materials science applications and practically by proposing GAMI-Net as a robust decision-support tool for frost-resistant concrete design.

Future research should address data limitations, extend interpretability frameworks to time-dependent degradation, and explore uncertainty quantification for broader real-world deployment.

Keywords: concrete; machine learning; interpretability; feature importance analysis; visualization; freeze-thaw resistance

1. Introduction

Machine learning (ML) serves as a vital component of artificial intelligence (AI), capable of identifying critical patterns within complex datasets to drive advancements across industries [1,2]. In civil engineering, ML has significant applications in structural health monitoring, concrete mix design optimization, and material behavior prediction modeling [3,4]. ML algorithms like decision trees [5], support vector machines [6], and random forests [7] have demonstrated practical value in construction workflows. These algorithms could assist engineers in distilling actionable insights from expansive datasets, enabling refined material selection and design strategies. For example, Luckey *et al.* [8] highlighted the integration of ML within smart city frameworks, with specific reference to its enhancement of civil engineering processes. Van Quan Tran *et al.* [9] applied artificial neural network (ANN) and cuckoo search methods to predict the compressive strength of recycled concrete based on a large amount of experimental data in the literature. Endzhievskaya [10] used random forests and decision tree algorithms to study the influence of concrete composition on the physical-mechanical properties of road concrete, where the most important factor affecting concrete structural strength was the coarse aggregate, whose size normally ranges from 5mm to 20 mm. Al Musawi *et al.* [11] used the support vector regression with firefly optimization algorithm (SVR-FFA) to predict the shear strength in steel fiber-reinforced concrete (SFRC) beams, analyzing geometric parameters and reinforcement mechanical properties. Their findings indicate the model effectively estimates structural shear capacity. Su *et al.* [12] explored chloride ion distribution in basalt-polypropylene fiber-reinforced concrete (BPFRC) under salt fog conditions, evaluating strength, fiber ratios, and mixing techniques. Experimental data revealed that 0.1% fiber content reduced chloride resistance, whereas 0.2% fiber inclusion elevated chloride concentrations within the composite material.

However, ML algorithms increasingly focus on operational decision-making, exposing a core limitation, such as the inherent lack of interpretability in their decision-making mechanisms. While these models demonstrate strong predictive performance, relying on them without understanding their internal logic can lead to predictions that lack alignment with the underlying material physics. For example, high feature importance assigned to parameters like curing time may obscure factors such as hydration kinetics. Traditional models often operate as “black boxes”, providing little or no interpretation of their internal decision-making process [13]. This opacity becomes critical in engineering disciplines that require transparent and logical decision, particularly civil engineering. [14]. Despite advancements in ML applications for civil engineering, model interpretation still remains a barrier to practical deployment. The rise of explainable AI (XAI) addresses this issue by decoding complex decision networks through systematic internal logic and operational patterns. It has been reported that XAI bridges computational accuracy and human analysis through interpretable algorithms that clarify conclusion formation [15,16]. In civil engineering, XAI could convert ambiguous predictions into reliable frameworks which are crucial when infrastructure reliability requires a traceable decision path.

Its transparency can enable engineers, project managers, and supervisors to understand the prediction process [17], making it possible to establish safe and reliable decisions.

Transparent predictive methods are crucial for assessing concrete's dynamic elastic modulus and frost resistance, particularly in environments prone to severe climatic fluctuations [18,19]. In cold regions, infrastructure is frequently exposed to freeze–thaw cycles, which progressively compromise structural integrity and reduce service life [20,21]. Accurate evaluation of the elastic modulus enables effective monitoring of material degradation and durability performance [22]. However, many conventional algorithms provide limited insight into how input parameters, such as mix proportions, curing conditions, or environmental conditions, influence predictions. This opacity restricts their value for materials engineering applications. To address this limitation, it is essential to employ models that not only predict performance accurately but also reveal the underlying relationships among variables. For example, elucidating how hydration kinetics interact with freeze–thaw effects can inform the optimization of concrete mix designs. Such interpretability not only enhances the reliability of model outputs but also supports the development of more durable, cost-effective concrete for cold climate applications.

XAI development prioritizes techniques that decode how models generate predictions and untangle complex computational processes. Dominant approaches include SHapley Additive exPlanations (SHAP) [23] and Local Interpretable Model-agnostic Explanations (LIME) [24]. These frameworks dissect input variable impacts on prediction outcomes through detailed interpretations. These methods could equip practitioners to manage model complexities, ensuring reliable and rational outcomes [25]. For example, Cui *et al.* [26] employed SHAP to analyze household and building features, quantifying their contributions to residential energy consumption patterns across the United States. Notably, XAI's capabilities extend beyond material property evaluation, to addressing diverse challenges in civil engineering through interpretable computational analysis. Elhishi *et al.* [27] demonstrated how XAI clarifies intricate predictive models for concrete strength estimation, establishing systematic frameworks for science-driven material validation and certification protocols. The adaptability of XAI extends to earthquake risk evaluation. For instance, Jena *et al.* [28] studied how interpretable models could uncover seismic event likelihood patterns to guide proactive infrastructure planning and urban design strategies. Similarly, Zhan *et al.* [29] introduced counterfactual explanations within XAI paradigms to strengthen risk-informed decision-making in construction management. A comprehensive analysis of current XAI research in civil engineering highlights its transformative potential across the field. In summary, XAI can enhance design quality, safety, and sustainability in civil engineering projects.

Remarkably, XAI has demonstrated significant potential for predicting concrete performance in civil engineering. Chakraborty *et al.* [30] analyzed the compressive behavior of high-performance concrete by calculating Shapley values to quantify feature contributions toward individual predictions. Zhao *et al.* [31] developed an integrated ML framework combining predictive and explanatory capabilities, enabling simultaneous assessment of compressive strength and flowability in cement-based grouting materials. Zeng *et al.* [32] explored the role of deep learning for interpretive features in the development of concrete strength and the interactions between various features in influencing concrete performance. Cakiroglu *et al.* [33] employed seven different ML models to predict the axial compression capacity of concrete-filled steel tubular columns, providing explanations for each model's predictive outcomes. Kulasooriya *et al.* [34] utilized ML to predict the compressive, tensile, and flexural strength of basalt fiber-reinforced concrete and employed XAI methods to illuminate these

predictions. Aladsani *et al.* [35] applied explainable ML techniques to assess the bond strength between concrete and corroded reinforcement, as well as the service and structural performance of corroded RC components. Indeed, XAI holds considerable advantages in elucidating the intricate relationships between materials and structural performance within concrete structural engineering. Similarly, the frost resistance of concrete is also affected by complex factors such as moisture content, water-cement ratio, aggregate size, and the number of freeze-thaw cycles [36–38]. Given the critical impact of frost damage on structural integrity and longevity, especially in colder climates, obtaining accurate predictions is not just an academic interest but also a practical necessity [39,40]. Although XAI provides transparency in model decision-making, the variety of inherent explanatory models to post-hoc explanation tools and their respective strengths and weaknesses requires further clarification. Therefore, a thorough analysis of the interpretability capabilities of these methods is crucial to ensure the effective application of XAI in real-world scenarios. Despite the recent application of XAI, there are still some limitations. First, many studies failed to fully consider the trade-off between model accuracy and interpretability when interpreting models, making it difficult to find a balance point in practical applications. Second, the datasets used in previous studies often have limitations and cannot fully reflect the complexity of concrete performance [41–48]. Table 1 summarizes previous studies of different XAI applications for predicting concrete materials.

Table 1. Comparison of key studies on explainable XAI applications in predicting concrete properties.

Study	Material type	Target property	XAI methods	Key findings
[30]	High-performance concrete	Compressive strength	SHAP	Identified key features affecting compressive strength, providing local explanations for each instance.
[31]	Cement-based grouting materials	Compressive strength, flowability	Integrated ML with SHAP	Developed a hybrid XAI framework to explain variations in cementitious material properties.
[32]	Concrete	Compressive strength	Deep learning + SHAP	Used deep learning models with XAI to reveal feature interactions in predicting concrete strength.
[33]	Concrete-filled steel tubular columns	Axial compression capacity	Multiple ML models + SHAP	Compared seven ML models and explained their predictive performance using SHAP.
[34]	Basalt fiber reinforced concrete	Compressive, tensile, and flexural strength	Multiple XAI methods	Developed a graphical interface for practical use of XAI in predicting concrete properties.
[35]	Reinforced concrete walls	Drift capacity	Explainable ML	Applied XAI to assess the bond strength and structural performance of corroded RC components.
This study	Concrete (Freeze-thaw experiments)	Elastic dynamic modulus	GAMI-Net, EBM, SHAP, LIME, Shapash	Compared multiple XAI models, highlighting GAMI-Net's advantage in interpretability and predictive performance.

Given the above, this study aims to conduct a comprehensive comparative analysis of five XAI methods: GAMI-Net, EBM, SHAP, LIME, and Shapash, for predicting the elastic dynamic modulus of concrete subjected to freeze–thaw cycles. Specifically, three predictive methods were employed: GAMI-Net and EBM, which are intrinsically interpretable, and XGBoost, a high-performing method whose outputs were interpreted using the post-hoc tools SHAP, LIME, and Shapash. The interpretability of these methods is evaluated from multiple perspectives, including transparency model training, prediction accuracy, feature importance rankings, and global, local, and dependency-based explanations. By comparing both inherently interpretable models and post-hoc explanation frameworks, this study aims

to identify the most effective and practically applicable tools for transparent prediction of concrete performance. The findings are expected to support the selection of interpretable machine learning methods in civil engineering, contributing to more reliable, explainable, and physically grounded decision-making in material design and durability assessment.

2. Methodology

2.1. Explainable methods

This study employs three distinct machine learning algorithms for prediction: GAMI-Net [49], EBM [50], and XGBoost [51]. GAMI-Net and EBM are inherently interpretable models, designed with transparent internal structures that reveal their decision logic. In contrast, XGBoost is a widely adopted high-performance algorithm that lacks built-in interpretability. To address this limitation, three post-hoc interpretability frameworks are applied specifically to the trained XGBoost model: SHAP [23], LIME [24], and Shapash [52]. These tools are not predictive models themselves; rather, they are used to analyze and explain the output of complex, opaque models. This approach enables a direct comparison between inherently interpretable models such as GAMI-Net and EBM, and XGBoost enhanced with post-hoc explanations, providing a comprehensive assessment of interpretability across different methodological approaches.

2.1.1. GAMI-Net

The GAMI-Net model, developed by Yang *et al.* [49], integrates structured interactions with generalized additive models using an explainable neural network (xNN) architecture [53]. It explicitly models the main effects and selected pairwise interactions using structured subnetwork components, each assigned learnable parameters that contribute to the final prediction. Interconnected subnetworks composed of input nodes effectively capture these additive and interactive effects, which are then aggregated to generate the output. GAMI-Net enhances interpretability through intuitive visualizations such as single-variable plots and interaction heatmaps. Its ability to deliver accurate predictions while maintaining transparency sets it apart from traditional black-box models and other interpretable frameworks [54].

The interpretability of the GAMI-Net model is driven by three embedded constraints: sparsity, heritability, and marginal clarity, implemented through a structured three-phase training process [49]. In the first phase, the model trains, normalizes, and prunes the subnetworks corresponding to main effects. The second phase identifies and fits the most significant pairwise interaction subnetworks, followed by pruning to reduce model complexity. The final phase jointly fine-tunes all remaining main effects and interactions to optimize performance. These constraints and phased training steps collectively enhance interpretability by clarifying the relationships between input variables and their combined effects. This design not only improves the identifiability of key predictive factors but also maintains high prediction accuracy without sacrificing model transparency [55].

GAMI-Net derives interpretability from the Importance Ratio (IR) of main effects and pairwise interactions, quantifying each variable's contribution to predictions [56]. The framework employs visualization tools such as partial dependence plots, single-axis graphs, and interaction heatmaps. Local interpretations further decode decision logic for individual instances. These features collectively expose the model's decision logic, variable significance, and prediction rationale.

2.1.2. EBM (Explainable Boosting Machine)

The Explainable Boosting Machine (EBM [50]) merges the Generalized Additive Model (GAM [57]) with gradient boosting via shallow decision trees [58] to address variable relationships. This framework precisely quantifies the main effects and interactions in interpretable models. EBM adjusts hyperparameters to rank variables and prioritizes critical ones during computation, establishing feature importance. Leveraging these techniques, the model generates predictions by leveraging estimated main effects and pairwise interactions.

EBM's inherent interpretability stems from its main effects and interaction shape functions, which provide intuitive visualizations of how individual variables and their combinations correlate with predictions [59]. EBM model offers both global and local interpretations for its decision logic and outcomes. Global interpretation examines population-level patterns by tracking variables' collective impact across datasets, while local interpretation queries individual variables' influence on single predictions. These interpretability features enable granular understanding of EBM's predictions at multiple scales, making it valuable across domains requiring transparent analytical frameworks.

2.1.3. XGBoost

XGBoost [51] enhances the Gradient Boosting Decision Trees (GBDT) with parallelized tree boosting algorithms, accelerating training and prediction speeds. Its optimized framework maintains accuracy while accelerating iterative refinement, driving broad adoption in applied ML scenarios [60]. Regularization constraints are embedded into the objective function to streamline model architecture and mitigate overfitting.

2.1.4. SHAP (SHapley Additive exPlainations)

Lundberg and Lee [23] proposed the SHAP (SHapley Additive exPlanations) algorithm, interpreting ML model outputs through cooperative game theory principles. SHAP constructs an additive model using Shapley values from game theory, bridging game theory with local explanations. The algorithm quantifies each feature's contribution to predictions across datasets. For each prediction sample, the model generates a prediction value, and the calculation formula for the Shapley value is as in Equation (1).

$$\phi_i(v) = \sum_{S \subseteq N \setminus \{i\}} \frac{|S|!(|N|-|S|-1)!}{|N|!} (v(S \cup \{x_i\}) - v(S)) \quad (1)$$

Where S is a subset of features used in the model, x is the vector of feature values for the instance being explained, N is the number of features, and $v(S \cup \{i\})$ represents the prediction of subset S with the inclusion of feature xi.

2.1.5. Local Interpretable Model-agnostic Explanations (LIME)

Ribeiro *et al.* [24] introduced the Local Interpretable Model-agnostic Explanations (LIME) algorithm to produce local explanations for ML model predictions. As a post-hoc interpretability technique, LIME builds an interpretable model around related predictions, and its local behavior is similar to that of

complex models. LIME compares the approximation between the explainable model g and the original model f by minimizing a loss function. The mathematical expression is as Equation (2).

$$\text{explanation}(x) = \text{argmin}_{g \subseteq G} L(f, g, \pi_x) + \Omega(g) \quad (2)$$

Where Ω(g) represents the model complexity of the explanatory model g, G denotes all possible explanatory models, and defines the neighborhood of x.

2.1.6. Shapash

Shapash is an overlay package specifically designed for model interpretability [52]. It utilizes the Shap backend to compute feature contributions. Shapash relies on different steps required to build a ML model to make the results easily understandable. It provides visualizations for both global and local interpretability, which can be applied to regression, binary classification, or multiclass classification problems. With Shapash, data scientists can easily understand their models and share their results, while users can use the most influential summaries to comprehend the decisions made by the model. Furthermore, it contributes to data science analysis by displaying useful information about the model and data within reports. Based on SHAP and LIME, Shapash serves as a convenient and fast method for interpretability.

2.2. Dataset

This study compiled 347 concrete test records from experimental investigations and published studies [43,47,61,62]. Each entry includes material constituents, cement; blast-furnace slag (BFS); fly ash; mixing water; air-entraining agent (AEA); superplasticizer (SP); fine aggregate (FA); and coarse aggregate (CA), together with the curing period (time, days) and the number of freeze–thaw (F-T) cycles, with statistical characteristics as detailed in Table 2. The output data Y represents the elasticity dynamic modulus of the concrete. Figure 1 presents a heatmap illustrating the Pearson correlation coefficients for various features, with values ranging between −1 and 1. The sign of the coefficient indicates the direction of the correlation, while its absolute magnitude signifies the strength of the relationship.

Table 2. Statistics of variables in the dataset.

Item	Unit	Mean	Standard deviation	Minimum	Median	Maximum
Cement	kg/m^3	401.45	140.44	262	380	875
BFS	kg/m^3	27.76	120.23	0	0	839
Fly Ash	kg/m^3	81.61	148.39	0	0	610.67
Water	kg/m^3	188.82	68.3	144	170	390.83
AEA	kg/m^3	0.04	0.19	0	0	2
SP	kg/m^3	0.31	1.28	0	0	6.7
CA	kg/m^3	558.92	502.19	0	665	1430
FA	kg/m^3	365.39	313.09	0	561.83	885
time	days	34.74	12.23	28	28	60
F-T cycles	times	102.79	89.69	0	91	400
Y	%	86.93	19.93	0	94.7	101.8

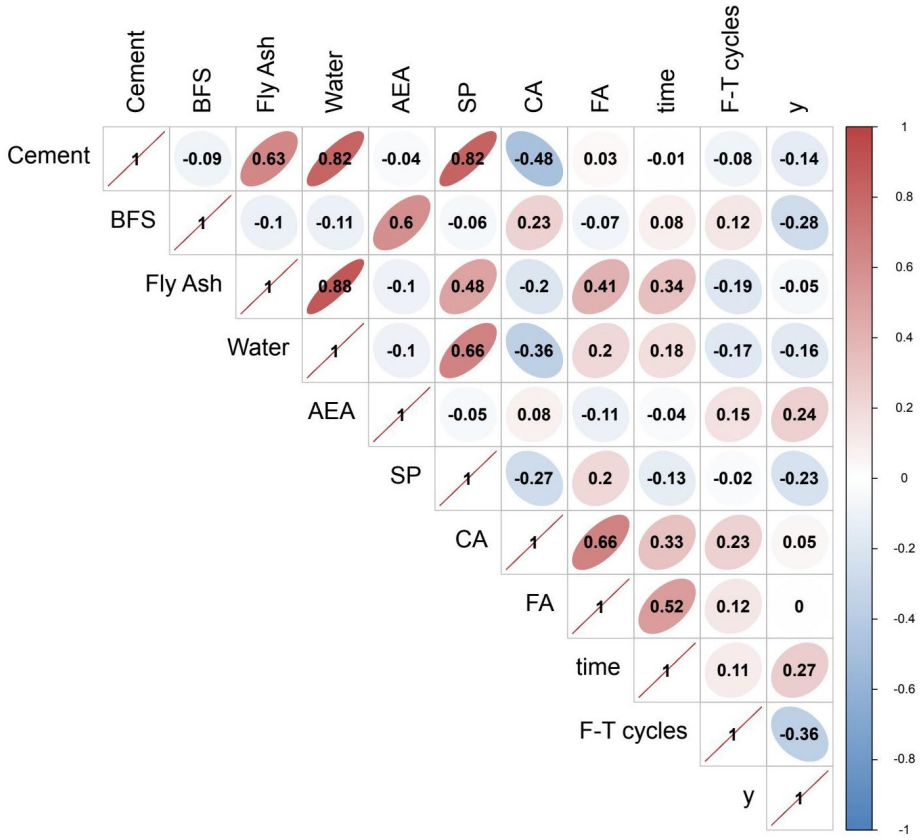

Figure 1. Pearson correlation coefficient of variables in the dataset.

2.3. Training process

The process of tuning in ML involves seeking optimal model performance through experimenting with various parameter combinations. Common tuning techniques include grid search [63], random search [64], and Bayesian optimization [65]. Across different tuning methods, the unified objective is to elevate model performance by iteratively fine-tuning parameters, selecting suitable metrics, allocating training time effectively, and employing cross-validation for robustness. This study adopted a grid search strategy to systematically identify optimal hyperparameter configurations. Specifically, the learning rate was configured at 0.0001, pairwise interaction terms were limited to 20, regularization parameters were set to 0.1, and the random seed was fixed at 3. By exhaustively evaluating predefined parameter combinations within specified ranges, grid search effectively locates the parameter set that maximizes model effectiveness. Detailed hyperparameter settings are shown in Table 3. Specifically, the GAMI-Net implementation was employed to optimize key parameters, including sparsity coefficients and learning rates. The optimization objective was formulated as minimizing the negative mean squared error (MSE) multiplied by 10, derived from cross-validation scores to emphasize performance stability.

Figure 3 illustrates the optimization of GAMI-Net, mapping the validation loss against the cumulative count of main effects and interactions. Red stars on the graph mark the points of minimum validation loss as new effects are added, suggesting optimal quantities for selection. Conversely, red circles denote the model's eventual choice of effects. Figure 3 visualizes GAMI-Net's training workflow, depicting the model's irrelevant effect pruning process. The illustration highlights interpretability during training phases, providing a transparent framework that differentiates it from other models.

Table 3. Hyperparameter settings.

Model	Hyperparameter	Search range	Final value
GAMI-Net	Learning rate	0.00001~ 0.1	0.0001
GAMI-Net	Pairwise interactions	10~30	20
GAMI-Net	Regularization	0.01~0.5	0.1
GAMI-Net	Random seed	Fixed	3
XGBoost	Tree depth	4-8	6
EBM	Learning rate	0.00001-0.1	0.01

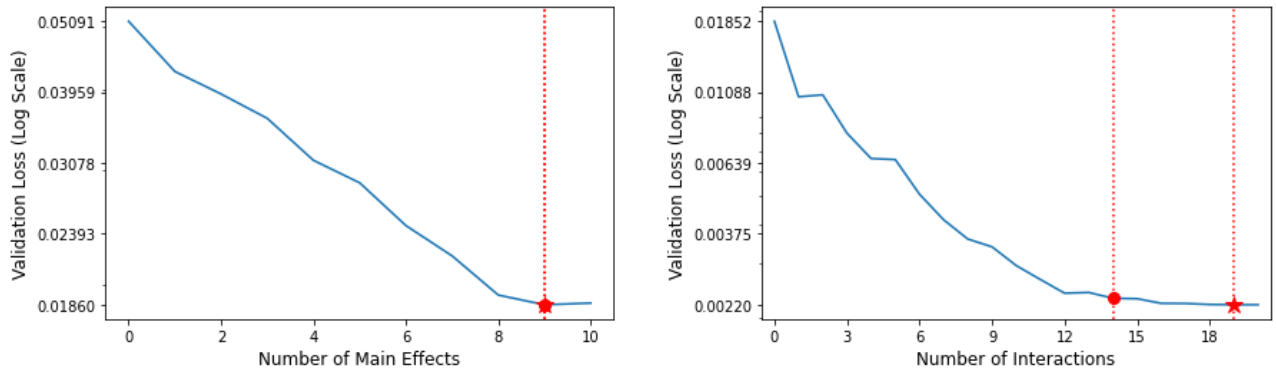

Figure 3. Determining the validation loss of the GAMI-Net model synthesis function. **(a)** Selection of the number of main effects; **(b)** Selection of the number of interactions.

EBM optimizes performance by adjusting learning rates, balancing parameter update speed with training stability. A lower learning rate stabilizes the model but slows convergence. A higher rate risks instability. Tuning involves testing varied learning rates and regularization terms to prevent overfitting. EBM initializes parameters, selects problem-specific energy functions, and defines optimization algorithms. Iterative computations refine parameters until preset convergence criteria are satisfied. The loss function derives from the energy function, minimizing sample energy by reducing loss penalties while suppressing noise interference. This iterative refinement sharpens the model's predictive accuracy.

XGBoost optimizes through feature subsampling and hyperparameter tuning, such as learning rate, number of trees, tree depth, and regularization parameters. During training, the framework iteratively builds and refines decision trees via gradient boosting. Early stopping prevents overfitting. Adapting loss functions aligns with problem-specific needs. This tuning enhances model robustness and sharpens predictive accuracy.

GAMI-Net, EBM, and XGBoost use distinct parameter-tuning approaches. Each framework exhibits unique strengths and constraints. GAMI-Net enhances interpretability through sparsity constraints, though this introduces complexity into parameter tuning. EBM stabilizes convergence via predefined energy functions, yet selecting optimal functions remains non-trivial. XGBoost leverages cross-validation and early stopping to boost efficiency and prevent overfitting, though its expanded hyperparameter space increases computational demands during optimization. Despite these challenges,

the iterative and adaptive nature of each model's tuning methodology effectively balances simplicity with predictive capability.

3. Results

3.1. Model accuracy evaluation

A 10-fold cross-validation strategy was employed to ensure robust performance evaluation. The RMSE and R^2values reported in Figure 4 represent the average across all folds, with standard deviations provided to quantify variability. To standardize goodness-of-fit assessment, this study prioritized RMSE due to its sensitivity to outliers in material property prediction, supplemented by R^2 for variance explanation. This dual-metric approach avoids reliance on subjective judgment. The analysis presented in Figure 4 showcases the predictive capabilities of the three ML models. The R^2 values, 0.95 for GAMI-Net, 0.97 for EBM, and 0.96 for XGBoost, demonstrate that all models explain a substantial proportion of the variance in the test sets, affirming their effectiveness in capturing the underlying data patterns. However, when examining the root mean square errors (RMSE), there's a notable disparity. GAMI-Net's RMSE of 0.04 is significantly lower than that of EBM(3.36) and XGBoost(3.99). EBM and XGBoost produce reliable predictions. GAMI-Net achieves higher accuracy, which this possibly due to its ability to better generalize or leverage more suitable constraints for the given data.

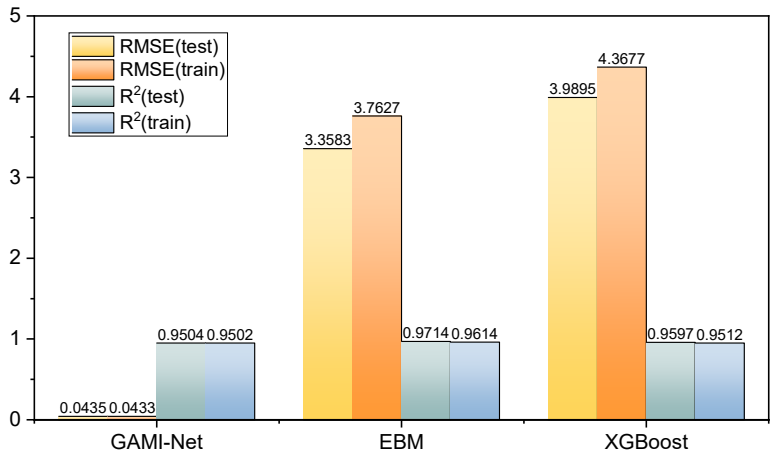

Figure 4. Prediction accuracy of three ML models.

3.2. Feature importance ranking

ML models generate feature importance rankings to clarify decision-making patterns. These rankings reveal how variables influence predictions. GAMI-Net identifies freeze-thaw cycles and water content as primary factors affecting concrete's dynamic elastic modulus (Figure 5a), aligning with experimental results. Increased freeze-thaw exposure degrades performance. Higher water content reduces modulus values. The model also quantifies secondary factors. Moderate slag content enhances durability, while excessive amounts weaken concrete properties. These insights validate model accuracy and guide material selection in engineering applications.

The overall interpretation of the GAMI-Net model, as shown in Figure 5a, systematically ranks main effects and pairwise interactions by evaluating each variable's predictive contribution through

importance ratios (IR). The vertical axis lists features, while the horizontal axis displays IR values normalized to sum to 1. The model ranks the significance of predictions based on their IRs. EBM calculates feature importance rankings based on calculating importance rankings through average contribution scores across training samples, as illustrated in Figure 5b. The horizontal axis quantifies each feature's predictive contribution, and the vertical axis orders features by descending contribution values. This also includes feature interactions, where the interaction between two features occurs after isolating individual contributions to the prediction. XGBoost's feature importance ranking is based on the number of times a feature is used for splitting across all trees, as depicted in Figure 5c. The ranking is done in descending order of importance. SHAP and Shapash calculate feature importance rankings based on the average absolute SHAP values of each feature. Figures 5d,e show the importance rankings of each feature from highest to lowest using SHAP and Shapash methods on an XGBoost model.

Figure 5a illustrates the main factors influencing the dynamic elastic modulus, with the paired interaction between water and freeze-thaw cycles and the number of freeze-thaw cycles being the primary influencing factor. In freeze-thaw tests, water and the number of F-T cycles are the main influencing factors, and excessive freeze-thaw cycles can cause significant damage to concrete. Therefore, the paired interaction of these two factors substantially impacts concrete's dynamic elastic modulus. Additionally, an increase in the number of F-T cycles leads to a decrease in the concrete dynamic elastic modulus. It should be noted that different outputs may have different rankings of input variable importance. Analyzing the importance of global features helps us understand the main factors influencing concrete performance and further analyze the prediction results. Table 4 presents the top ten important effects of the model outputs in the experiment. Both SHAP and Shapash adopt the same calculation method for importance, producing identical results. As shown in Table 4, in the experiment on dynamic elastic modulus, the major features identified by GAMI-Net are the combined interaction between F-T cycles and water, as well as the number of F-T cycles. For EBM, the primary features are the number of F-T cycles and the interaction term between water and F-T cycles. XGBoost highlights the importance of fine aggregate and air entrainment. SHAP identifies the number of freeze-thaw cycles and water as the primary features.

It can be observed that due to the different calculation methods for feature importance in each model, there are variations in the ranking of feature importance. However, the top-ranked features in each set of experiments are generally consistent. For example, in the experiment on dynamic elastic modulus, the number of F-T cycles, water, and blast furnace slag are identified as important factors affecting the corresponding concrete performance [66]. Therefore, each model can provide reasonably accurate results regarding the most influential features on the prediction outcomes. The importance of ranking may vary based on different criteria, often relying on researchers' personal experience. The feature importance ranking of the GAMI-Net model is calculated based on the contribution of each variable to the overall prediction. The calculation of importance ratios is based on the empirical distribution of explanatory variables rather than assuming that all variables are independent and uniformly distributed. This approach yields more reliable results. Moreover, GAMI-Net's importance ranking demonstrates strong consistency with real-world concrete behavior patterns. This preference for GAMI-Net is further supported by its structural design. Unlike tree-based models such as XGBoost, which rely on the frequency of feature splits across many decision trees, GAMI-Net assigns feature importance by modeling both main and interaction effects using an interpretable additive framework. This allows it to

better capture underlying dependencies between various variables, especially in concrete performances, which often result from the coupling of multiple factors. The stability of GAMI-Net's ranking is not only rooted in its algorithmic logic but also reflects its alignment with physical understanding, as observed in how it consistently highlights water content and F-T cycles as dominant features influencing the dynamic modulus performance of concrete. Such consistency makes it a reliable choice for feature importance analysis in engineering applications. Consequently, we choose to trust GAMI-Net's feature importance ranking in this study. Before model training, all input variables were standardized to enable a consistent basis for interpreting feature importance across different models.

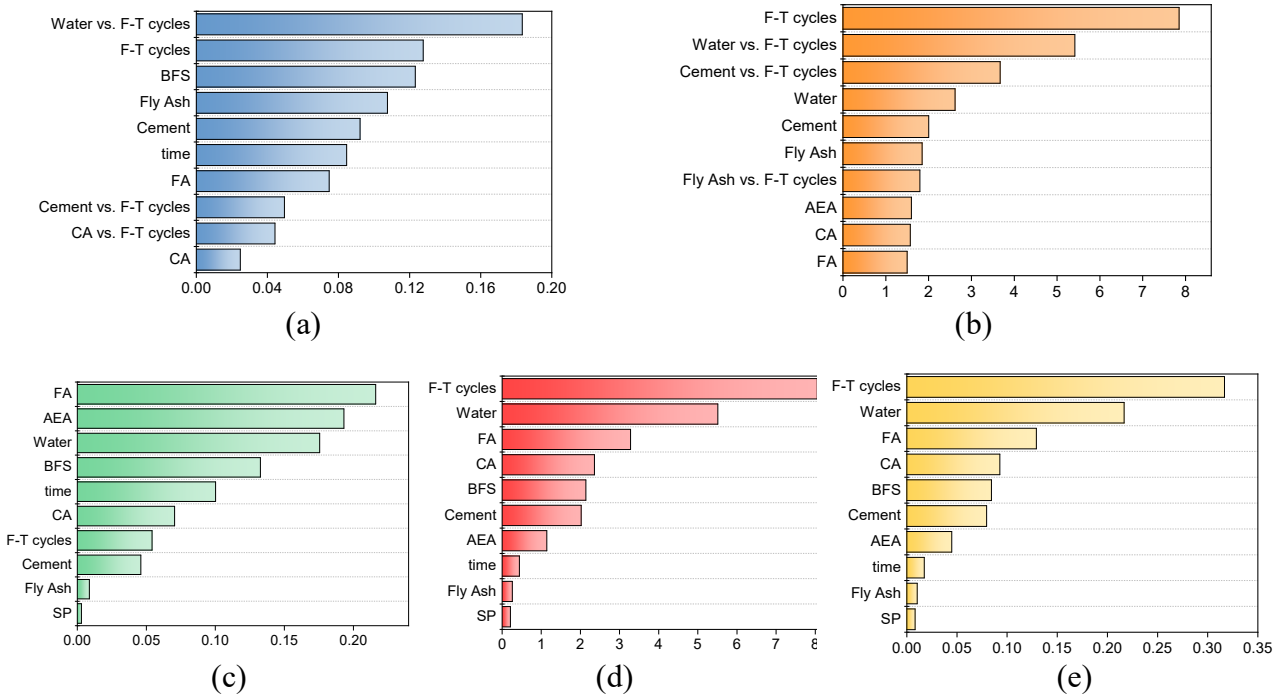

Figure 5. Feature importance ranking of the models. **(a)** GAMI-Net; **(b)** EBM; **(c)** XGBoost; **(d)** SHAP; **(e)** Shapash.

Table 4. Rank of characteristic importance of elasticity dynamic modulus.

Rank	GAMI-Net	EBM	XGBoost	SHAP/Shapash
1	Water *vs.* F-T cycles	F-T cycles	FA	F-T cycles
2	F-T cycles	Water *vs.* F-T cycles	AEA	Water
3	BFS	Cement *vs.* F-T cycles	Water	FA
4	Fly Ash	Water	BFS	CA
5	Cement	Cement	time	BFS
6	time	Fly Ash	CA	Cement
7	FA	Fly Ash *vs.* F-T cycles	F-T cycles	AEA
8	Cement *vs.* F-T cycles	AEA	Cement	time
9	CA *vs.* F-T cycles	CA	Fly Ash	Fly Ash
10	CA	FA	SP	SP

3.3. Global interpretation

Furthermore, GAMI-Net produces partial dependence visualizations. Single-variable relationships in main effects are displayed through linear graphs, while dual-variable interaction effects are represented using heatmaps. As shown in Figure 6, in linear plots, vertical coordinates quantify feature contributions to predictions, with horizontal positions indicating feature variables. Heatmaps arrange primary interaction variables horizontally, with secondary variables plotted vertically to visualize combined influences. Heatmap color gradients directly correlate with interaction significance, where elevated luminosity levels denote stronger combined variable influences on prediction outcomes. In the graph, each main effect or pairwise interaction is arranged in descending order of importance.

Figure 6 shows GAMI-Net's global interpretation for predicting concrete's dynamic elastic modulus. It can be observed that an increase in F-T cycles leads to a reduction in the concrete's dynamic elastic modulus, aligning with established experimental findings on F-T concrete behavior [62,66,67]. The inclusion of a small amount of blast furnace slag slightly improves the performance of concrete, while excessive inclusion results in a decrease in performance [68]. With the increase of fly ash content, the concrete dynamic elastic modulus increases first and then decreases. Fly ash content can improve the workability of the concrete mixture and reduce the required mixing water, thus increasing the concrete dynamic elastic modulus to some extent while maintaining concrete strength. However, excessive addition of fly ash reduces the water-to-cement ratio and decreases the performance of concrete [69]. In summary, GAMI-Net's global interpretation allows for clarification of the impact of main factors on the prediction results and provides insights into the correlations between various variables and the performance of concrete.

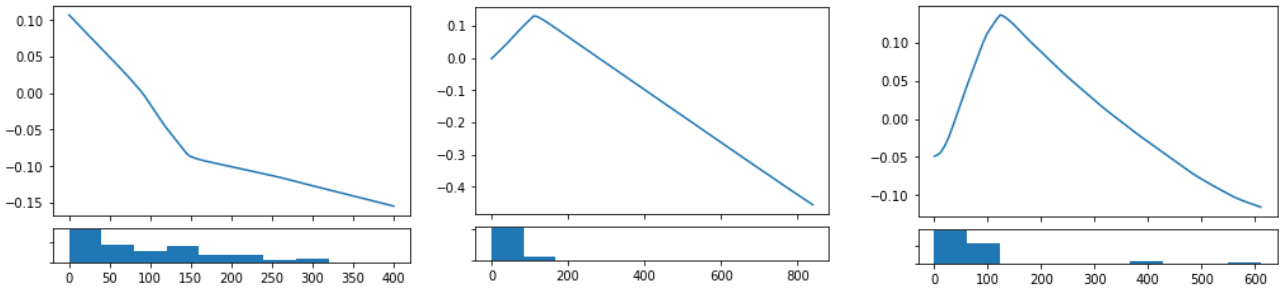

(a) (b) (c)

Figure 6. Global interpretation of the GAMI-Net model. **(a)** F-T cycles ;**(b)** BFS; **(c)** Fly Ash.

EBM, SHAP, and Shapash can also provide global explanations for predictive results. As shown in Figure 7, EBM provides global explanations by selecting some of the top main effects based on their feature importance rankings. For each effect, the line plot above shows the feature's contribution, where the gray band represents the prediction accuracy. The corresponding bar chart below represents the data distribution of the variable, and the trend analysis of each feature's impact on the prediction result can be derived from analyzing the line plot.

Figure 8a illustrates the global explanation using SHAP. Each row represents a feature, and the *x*-axis represents the SHAP value. Each point represents a sample, and the color indicates the feature value (red for high, blue for low). For example, in Figure 8a, there is a negative correlation between water and freeze-thaw cycles and elasticity dynamic modulus. The global explanations provided by SHAP are

consistent with those provided by GAMI-Net. In the interaction plot shown in Figure 8b, the diagonal represents the main effect of a particular feature, while the off-diagonal elements represent the pairwise interaction effects between the feature and other features. The focus is mainly on the diagonal, which helps explain the relationship between individual features and the label. In each subplot, the *x*-axis represents the SHAP value, with each point representing a sample. The number of samples is stacked vertically, and the color represents the feature value corresponding to the vertical line. Taking the first row as an example, the sum of the SHAP values across the entire row represents the SHAP value of that feature.

Figure 7. Global interpretation of the EBM model. **(a)** F-T cycles; **(b)** Water; **(c)** Cement; **(d)** Fly Ash.

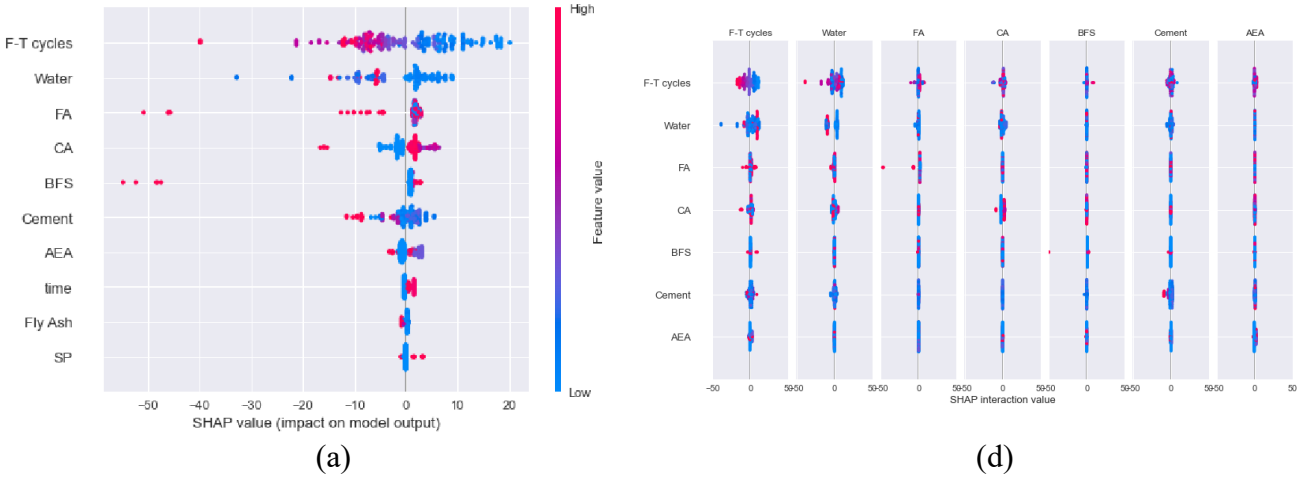

Figure 8. Global interpretation of the SHAP model. **(a)** Global explanation; **(b)** Interaction plot.

Figure 9 shows the global explanation using Shapash. Each point represents a sample, and the color depth of the sample point represents the magnitude of the predicted value. The *x*-axis represents the number of effects, and the y-axis represents the impact of each effect on the prediction result in the corresponding sample. The trend analysis of each feature's impact on the prediction result can be derived from the distribution trend of the sample points. Shapash treats features such as curing time and coarse aggregate,

which have concentrated data distributions, as categorical variables. The distribution trend of sample points follows the same principle as SHAP, but compared to SHAP, where the trend can only be determined by color changes, the trend plot of sample points in Shapash is more intuitive and easier to analyze.

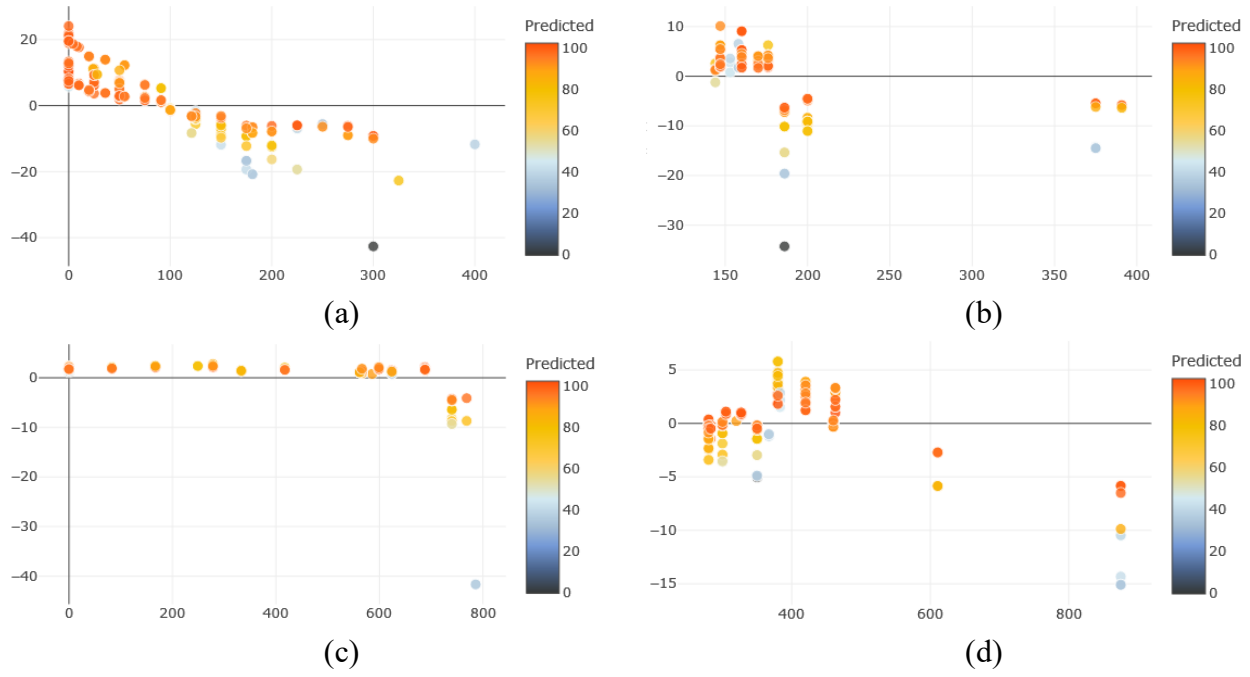

Figure 9. Global interpretation of the Shapash model. **(a)** F-T cycles; **(b)** Water; **(c)** FA; **(d)** Cement.

By comparison, the sample-based global explanations provided by SHAP and Shapash can reveal the relationship between each effect and the prediction result. However, when there is missing data for certain features, they may not provide reliable explanations. On the other hand, the one-dimensional line plots and two-dimensional heatmaps provided by GAMI-Net are easier to understand compared to the global explanations of SHAP and Shapash. They allow for a more intuitive and rapid analysis of the prediction results. Although EBM can provide explanations like GAMI-Net, it exhibits significant fluctuations when the prediction results undergo substantial changes, and it struggles to explain such situations. For example, in Figure 7, it is difficult to directly understand the variation trend of elasticity dynamic modulus with the amount of water from the line plot. In contrast, due to its smooth and continuous fit model, GAMI-Net does not encounter these issues. Additionally, the main effects and pairwise interactions selected by GAMI-Net are automatically pruned by the model, which simplifies the complexity of the model and further improves its interpretability. In addition to its visual interpretability, the algorithmic design of GAMI-Net also plays a key role in its advantage for global explanation in this study. Unlike models that rely only on post-hoc analysis, GAMI-Net inherently embeds interpretability into its architecture by modeling additive and pairwise interactions in a structured and continuous manner. This design ensures that feature effects are captured as smooth and coherent functions, making it easier to trace meaningful trends across varying input parameters. Particularly in concrete performance-related problems, where nonlinear behavior arises from multiple interdependent variables, the ability to preserve stable global patterns becomes essential. As seen in Figure 6, the monotonic and smooth profiles generated by GAMI-Net align well with physical expectations, avoiding the abrupt transitions observed in EBM or the point-based scatter of SHAP. This

stable trend is not simply an artifact of the modeling process, but a reflection of underlying material behavior. Therefore, in terms of global explanations, GAMI-Net is superior.

3.4. Local interpretation

GAMI-Net does provide local explanations for predictions by offering detailed contributions of individual variables to a single prediction. For a given sample, based on the input values of the features, the model can generate the final decision and directly provide the values of each additive component, including main effects or pairwise interactions, ranked by importance. This allows for a specific understanding of the input's contribution to the decision.

Figure 10 illustrates the local interpretation for a test dataset sample point. In the figure, "Intercept" represents the intercept of the null model, which is the average value of the outcomes for all samples. All model inputs underwent standardization. High-impact features exert substantial influence on predictions, displaying the influence of individual features on the predicted values. In Figure 10, the actual normalized dynamic elastic modulus value is 0.9374, while the predicted value is 0.9342, demonstrating close alignment between computational outputs and empirical observations.

Figures 11 to 14 provide local explanations provided by several other explainable models, which can also explain the decision process of a specific sample point. Figure 11 shows the local explanation provided by EBM (Explainable Boosting Machine). The Intercept represents the average value of the sample's outcome. Similar to GAMI-Net, the features are sorted by the absolute value of their impact, showing each feature's influence on the predicted outcome. Figure 12 presents the local explanation provided by LIME (Local Interpretable Model-Agnostic Explanations). The left part of Figure 12 provides the range of predicted values and the predicted value with the highest possibility. The middle part shows the impact of each feature on the predicted outcome based on the average value, sorted by the absolute value of its impact. The right part displays the magnitude of each feature value. Figure 13 displays the local explanation provided by SHAP (SHapley Additive exPlanations). The color and direction of the arrows represent the direction of the effect, and the length represents the magnitude of the effect. The features are sorted by the absolute value of their impact. The explanation starts from the bottom and follows the direction of the arrows to reach the predicted value. $E[f(x)]$ represents the average predicted value of all samples, while $f(x)$ represents the predicted value of the specific sample. As illustrated in Figure 14, Shapash visualizes the local explanations of feature contributions to the prediction of a specific sample. The features are sorted in descending order based on their impact magnitude. The zero point on the horizontal axis represents the average baseline value of all samples, and the length and direction of the feature bars extending from this zero axis quantitatively reflect the degree of each feature's influence on the current sample's prediction. These explainable models offer different ways to understand the decision process and influencing factors of the model for a specific sample. They help us gain better insights into the model's predictions and provide corresponding explanations.

In the elasticity dynamic modulus test, GAMI-Net, SHAP, LIME, and Shapash all provide local explanations for this sample. Analysis revealed that water and cement concentrations consistently exerted substantial positive contributions to the predicted modulus values across methodologies. Additionally, F-T cycles emerged as the most detrimental factor with pronounced negative influence magnitudes. This agreement reinforces the credibility of the local interpretations. Cross-comparative analysis indicates that the local explanations are based on the average predicted outcome and the impact

of each feature on the prediction, sorted accordingly. While the key influencing factors are generally consistent across models, some differences in magnitude and ranking arise. These discrepancies mainly stem from the underlying mechanisms of each model. For instance, SHAP and Shapash use additive attribution methods based on a model based on small input variations that reveal how each feature influences the prediction, whereas GAMI-Net derives local explanations directly from the learned main and interaction effects. This allows GAMI-Net to preserve the local contributions of features within its interpretable architecture, potentially yielding more stable and physically aligned results.

The major influencing effects are similar across these models, with only a few differences. These differences arise due to variations in the calculation methods of different explainable models and the criteria for determining positive or negative impacts of the same input variables in different models. However, all these explainable models show similar effects in providing local explanations for a specific sample. LIME offers more aesthetically pleasing result visualizations, while Shapash is more user-friendly in terms of usability. The local explanations for all test samples in Shapash can be obtained by clicking on the sample points in the global explanation chart. In comparison, GAMI-Net's advantage lies in its ability to link local prediction behavior with the model's structured representation of main and pairwise effects. This not only improves transparency, but also supports domain interpretation, especially when applied to concrete materials whose responses depend on coupling parameters.

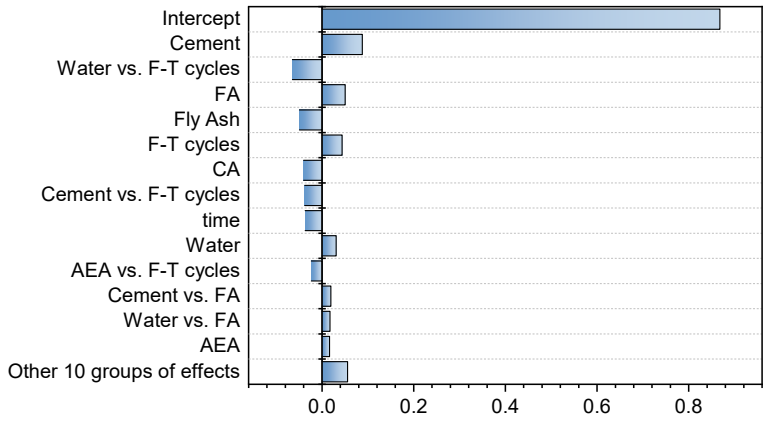

Figure 10. Local interpretation of the GAMI-Net model.

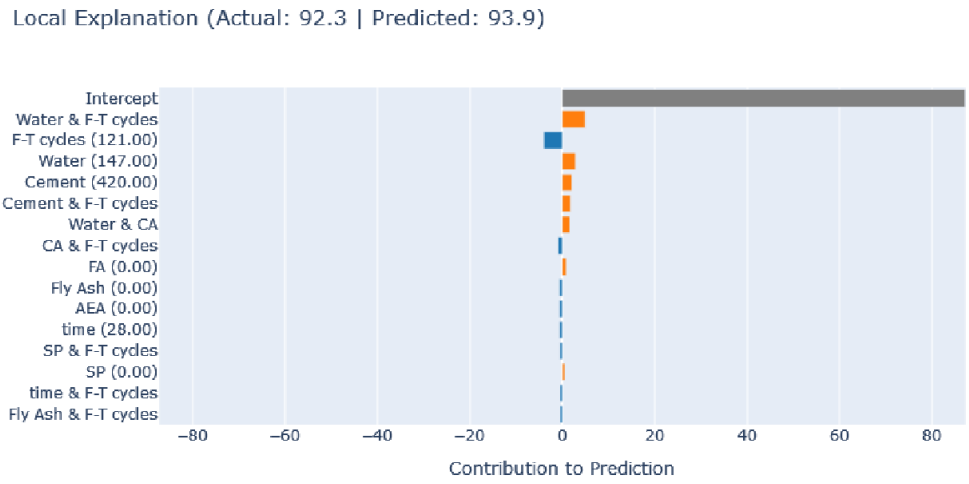

Figure 11. Local interpretation of the EBM model.

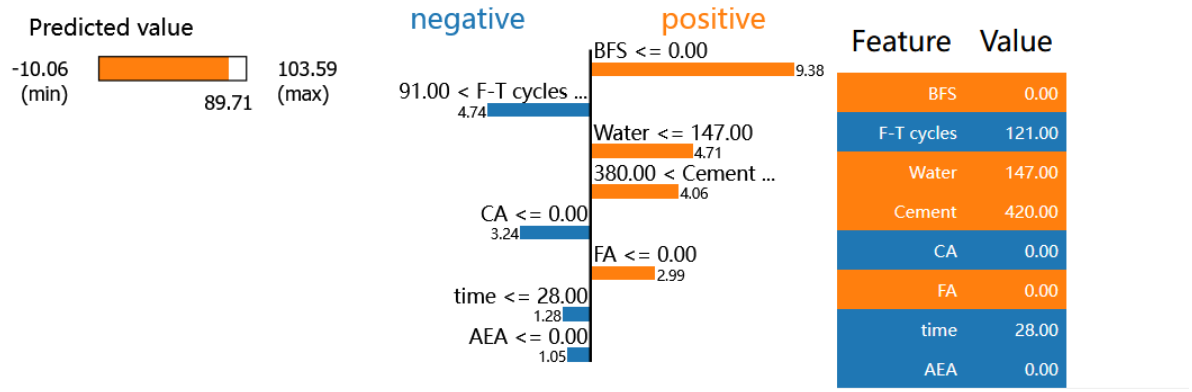

Figure 12. Local interpretation of the LIME model.

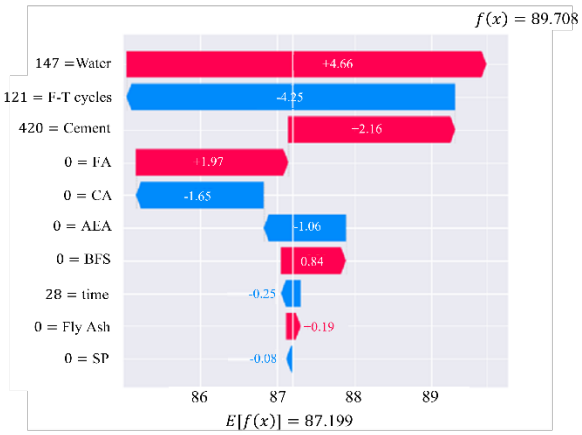

Figure 13. Local interpretation of the SHAP model.

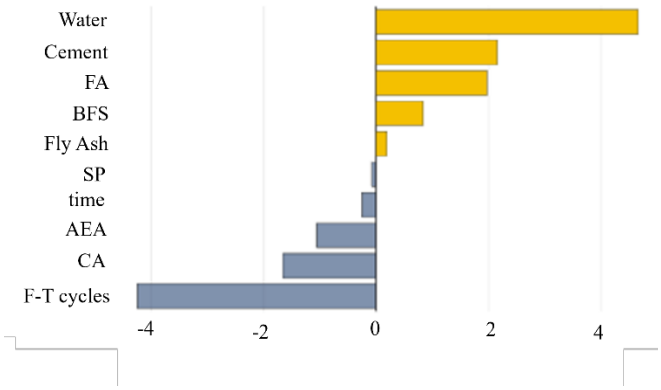

Figure 14. Local interpretation of the Shapash model.

3.5. Dependence interpretation

Some explainable ML models can also provide feature dependency graphs based prediction results. Figure 15 shows the dependency graph generated by GAMI-Net, which illustrates the joint effects of feature interactions on predictions. The interaction between F-T cycles and water indicates that increases in both variables lead to a decrease in the dynamic elastic modulus of concrete. Figure 16 presents the dependency graph generated by EBM, which exhibits similar effects to those of GAMI-Net. For these interaction terms, the x- and y-axes represent the values of the respective features, while the color depth reflects the impact of their interactions on prediction outcomes.

SHAP can also generate feature dependency plots. As shown in Figure 17a, the dependency between "Water" and "F-T cycles" is illustrated. Each point represents a sample, with the x-axis showing the feature values of "Water" and the y-axis showing the SHAP values of "Water," while the color scale represents the values of "F-T cycles." It can be observed that when the values of "F-T cycles" are lower (blue color), the influence of "Water" is weaker, as reflected by smaller SHAP values. This plot can be interpreted together with the global explanation plots by selecting the same axes for a consistent data representation. Figure 17b presents the dependency between "Cement" and "F-T cycles." Unlike the paired-effect analysis in GAMI-Net and EBM, SHAP's dependency plots focus on the marginal influence of one feature conditioned on another. These differences stem from the underlying model

mechanisms. GAMI-Net employs interpretable additive components with regularized smooth functions, ensuring continuity in variable interactions. By contrast, SHAP relies on sampled local approximations. In applications such as concrete performance prediction, where feature relationships often evolve smoothly with physical parameters, the heatmaps from GAMI-Net and EBM offer clearer representations of multivariate dependencies. Such visualizations are particularly valuable for identifying nonlinear effects or thresholds critical to structural degradation.

Through the comparison of feature importance rankings, global explanations, local explanations, and dependence explanations provided by different models, it is evident that GAMI-Net, which incorporates interpretability constraints such as sparsity, heredity, and marginal clarity, offers superior interpretability. These constraints not only guide the identification of critical predictive features but also ensure smooth and physically consistent representations at both global and local levels. As a result, GAMI-Net provides more reliable feature importance rankings, clearer global explanations, and refined local interpretations, thereby enhancing transparency in decision-making.

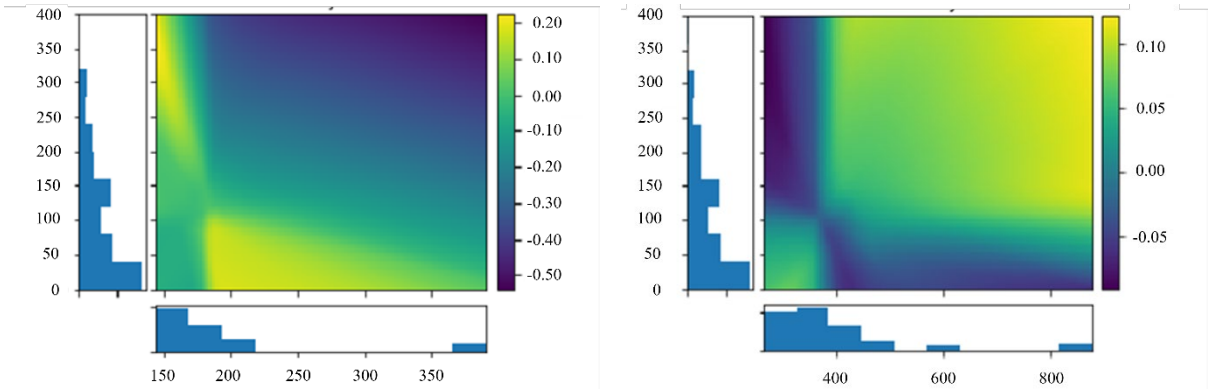

(a) (b)

Figure 15. The feature dependency graph provided by the GAMI-Net model. **(a)** Water *vs.* F-T cycles; **(b)** Cement *vs.* F-T cycles.

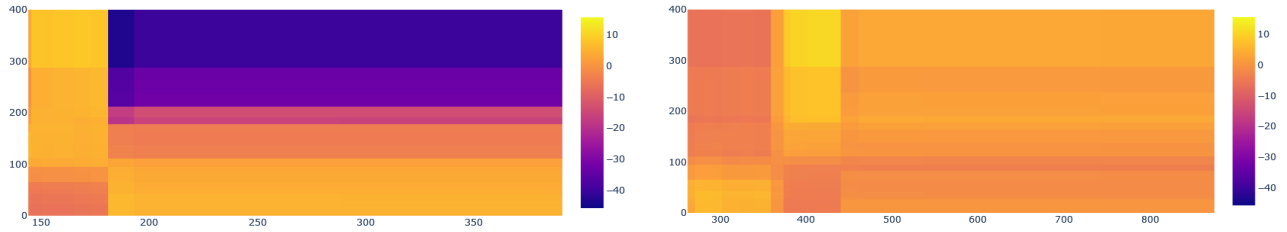

(a) (b)

Figure 16. The feature dependency graph provided by the EBM model. **(a)** Water *vs.* F-T cycles; **(b)** Cement *vs.* F-T cycles.

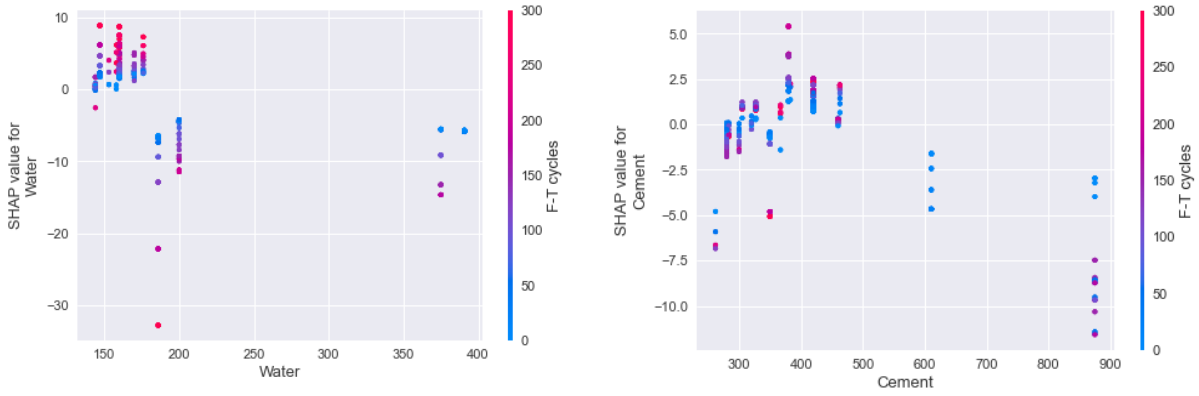

(a) (b)

Figure 17. The feature dependency graph provided by the SHAP model. **(a)** Water *vs.* F-T cycles; **(b)** Cement *vs.* F-T cycles.

The research has further evaluated model performance across both predictive accuracy and interpretability metrics. A summary of the basic functionalities of the employed models is presented in Table 5. Overall, the comparative analysis of GAMI-Net, EBM, and XGBoost (with SHAP, LIME, and Shapash) shows that while all models can achieve comparable predictive accuracy, their interpretability differs substantially. GAMI-Net consistently provided the clearest multilevel explanations (feature ranking, global, local, and dependence), with constraints such as sparsity and heredity ensuring stable and physically meaningful interpretations. EBM also offered reliable interpretability but exhibited fluctuations in highly nonlinear regions. SHAP supplemented XGBoost with valuable insights, though its local sampling occasionally obscured smooth physical relationships. These findings underscore the importance of balancing predictive accuracy with interpretability in civil engineering applications.

Table 5. Introduction to Explainable ML Models.

Models	Type	Predictive capability	Explainable capability			
			Feature importance ranking	Global interpretation	Local interpretation	Dependence interpretation
GAMI-Net	Generalized Additive Neural Network Model	✓	✓	✓	✓	✓
EBM	Linear Enhanced Learning Tree Model	✓	✓	✓	✓	✓
XGBoost	Gradient Boosting Decision Tree Model	✓	✓	--	--	--
LIME	Local Interpretable Model-Agnostic Explanations	--	✓	--	✓	--
SHAP	SHapley Additive exPlanations	--	✓	✓	✓	✓
Shapash	Python library for model interpretation	--	✓	✓	✓	--

4. Conclusion

In this study, three machine learning models, GAMI-Net, EBM, and XGBoost, were evaluated for their ability to predict the elastic dynamic modulus of concrete under freeze–thaw conditions. To enhance interpretability, three post-hoc explanation tools, SHAP, LIME, and Shapash, were applied to the XGBoost model. A dataset comprising 347 sets of concrete freeze–thaw test records was used, with input features including cement, BFS, fly ash, water, AEA, SP, FA, CA, curing time, and the number of freeze–thaw cycles. The interpretability of GAMI-Net and EBM, as inherently explainable models, was compared with that of the XGBoost model supplemented by SHAP, LIME, and Shapash. The conclusions are as follows:

(1) GAMI-Net achieved superior predictive accuracy in terms of RMSE (0.04), outperforming EBM (RMSE = 3.36) and XGBoost (RMSE = 3.99), while maintaining a high R^2 value of 0.95. EBM achieved a slightly higher R^2 value of 0.97 but with a much higher RMSE. GAMI-Net's structured training process and built-in constraints enabled the model to maintain high accuracy while offering smooth, transparent interpretations. Compared to SHAP and Shapash, which struggled under data sparsity or abrupt prediction transitions, GAMI-Net's explanations remained stable and physically aligned. EBM also provided robust explanations but exhibited noticeable fluctuations in highly nonlinear regions.

(2) Freeze–thaw cycles and water content are the most influential factors affecting the elastic dynamic modulus of concrete. Especially, the interaction between these features, especially under different cement and fly ash content, plays a critical role in predicting degradation. This aligns well with established physical behavior and highlights the models' ability to uncover meaningful material-performance relationships.

(3) The two-dimensional heatmaps generated by GAMI-Net and EBM provided more intuitive insights into feature interactions compared to SHAP-based scatter plots. These visualizations clarified how combined variables, such as water content and supplementary cementitious materials, nonlinearly influenced performance outcomes, thus enabling more informed engineering decisions.

The study offers both theoretical and practical contributions as follows. Theoretically, it demonstrates how intrinsically interpretable models can preserve physical realism in complex multivariable settings, bridging the gap between statistical learning and material science. Practically, it highlights GAMI-Net as a reliable decision-support tool for performance forecasting and mixing optimization in cold regions. This supports the development of robust, frost-resistant concrete formulations and enhances trust in ML-driven durability assessments in infrastructure design and maintenance. This supports the development of robust, frost-resistant concrete formulations and enhances trust in ML-driven durability assessments in infrastructure design and maintenance. This study highlights the inherent trade-off between predictive accuracy and interpretability. While black-box models with post-hoc explanations can achieve strong performance, intrinsically interpretable models such as GAMI-Net and EBM provide explanations that more closely align with physical mechanisms. Bridging this trade-off is essential for ensuring that machine learning predictions in civil engineering are not only statistically robust but also scientifically meaningful. Despite its strengths, the study has limitations. First, the dataset size may limit the generalizability of the findings across broader material systems or more diverse environmental exposures. Second, while GAMI-Net handles interactions effectively, the selection of interaction terms is still driven by empirical thresholds that may not capture

all nonlinearities. Additionally, the post-hoc methods applied to XGBoost are model-agnostic and may introduce inconsistencies when feature interdependencies are complex. Future work should expand the dataset by integrating multi-source experimental results and incorporating more robust uncertainty quantification methods. Furthermore, incorporating temporal freeze–thaw degradation dynamics and damage progression modeling could offer deeper insights into long-term durability under fluctuating environmental conditions. Furthermore, from a practical perspective, the deployment of interpretable ML models in civil engineering requires careful consideration of data availability, computational cost, and integration with existing engineering standards. For instance, real-world projects often involve incomplete or noisy monitoring data, which may limit the applicability of models trained on controlled laboratory datasets. In addition, the scalability of the proposed methods remains an open challenge. While this study demonstrates feasibility on a moderately sized dataset, extending these approaches to large-scale infrastructure networks or multi-modal sensing data will require more efficient algorithms and parallelizable training strategies. Addressing these challenges in future work is essential to ensure that interpretable ML frameworks can transition from experimental validation to reliable tools for large-scale engineering practice.

Acknowledgments

This work was funded by the Natural Science Foundation of Zhejiang Province (Grant No. LQ21E080017).

Authors' contribution

Haoyang Zheng: investigation, methodology, visualization, writing—original draft. Yuxiang Huang: data curation, investigation, review & editing. Kechang Wu: software, formal analysis, visualization. Bowen Wang: data curation, validation. Qingyuan Hu: investigation, review & editing. Dianchao Wang: formal analysis, methodology, review & editing. Bochao Sun: conceptualization, experiment, supervision, investigation, writing-original draft, project administration. Maxwell Fordjour Antwi-Afari: review & editing. All authors have read and agreed to the published version of the manuscript.

Conflicts of interests

The authors declare no conflict of interest.

References

[1] Naranjo-Pérez J, Infantes M, Fernando Jiménez-Alonso J, Sáez A. A collaborative machine learning-optimization algorithm to improve the finite element model updating of civil engineering structures. *Eng. Struct.* 2020, 225:111327.

[2] Turing AM. I. Computing machinery and intelligence. *Mind* 1950, LIX(236):433–460.

[3] Ke X, Duan Y. A Bayesian machine learning approach for inverse prediction of high-performance concrete ingredients with targeted performance. *Constr. Build. Mater.* 2021, 270:121424.

[4] Ahmad A, Ostrowski KA, Maślak M, Farooq F, Mehmood I, *et al*. Comparative study of supervised machine learning algorithms for predicting the compressive strength of concrete at high temperature. *Materials* 2021, 14:4222.

[5] Karbassi A, Mohebi B, Rezaee S, Lestuzzi P. Damage prediction for regular reinforced concrete buildings using the decision tree algorithm. *Comput. Struct.* 2014, 130:46–56.

[6] Harish N, Janardhan P. Support vector machine in predicting epoxy glass powder mixed cement concrete. *Mater. Today Proc.* 2021, 46:9042–9046.

[7] Li H, Lin J, Lei X, Wei T. Compressive strength prediction of basalt fiber reinforced concrete via random forest algorithm. *Mater. Today Commun.* 2022, 30:103117.

[8] Luckey D, Fritz H, Legatiuk D, Dragos K, Smarsly K. Artificial intelligence techniques for smart city applications. In *Proceedings of the 18th International Conference on Computing in Civil and Building Engineering*, São Paulo, Brazil, August 18–20, 2020, pp. 3–15.

[9] Quan Tran V, Quoc Dang V, Si Ho L. Evaluating compressive strength of concrete made with recycled concrete aggregates using machine learning approach, *Constr. Build. Mater.* 2022, 323:126578.

[10] Endzhievskaya IG, Endzhievskiy AS, Galkin MA, Molokeev MS. Machine learning methods in assessing the effect of mixture composition on the physical and mechanical characteristics of road concrete. *J. Build. Eng.* 2023, 76:107248.

[11] Al-Musawi AA, Alwanas AAH, Salih SQ, Ali ZH, Tran MT, *et al*. Shear strength of SFRCB without stirrups simulation: implementation of hybrid artificial intelligence model. *Eng. Comput.* 2020, 36:1–11.

[12] Su L, Niu D, Huang D, Luo Y, Qiao H, *et al*. Chloride diffusion behavior and microstructure of basalt-polypropylene hybrid fiber reinforced concrete in salt spray environment. *Constr. Build. Mater.* 2022, 324:126716.

[13] Mall PK, Singh PK, Srivastav S, Narayan V, Paprzycki M, *et al*. A comprehensive review of deep neural networks for medical image processing: recent developments and future opportunities. *Healthcare Anal.* 2023, 4:100216.

[14] Naser MZ. Causality in structural engineering: discovering new knowledge by tying induction and deduction via mapping functions and explainable artificial intelligence. *AI Civ. Eng.* 2022, 1:6.

[15] Lisboa PJG, Saralajew S, Vellido A, Fernández-Domenech R, Villmann T. The coming of age of interpretable and explainable machine learning models. *Neurocomputing* 2023, 535:25–39.

[16] Liang Y, Li S, Yan C, Li M, Jiang C. Explaining the black-box model: a survey of local interpretation methods for deep neural networks. *Neurocomputing* 2021, 419:168–182.

[17] Abadía JJP, Fritz H, Dadoulis G, Dragos K, Smarsly K. Automated decision making in structural health monitoring using explainable artificial intelligence. In *28th International Workshop on Intelligent Computing in Engineering (EG-ICE)*, Berlin, Germany, June 30, 2021, pp. 432–441.

[18] Sun B, Zheng H, Zhao Q, Zhao W, Fu W, *et al*. Enhancing concrete frost resistance prediction with an explainable neural network. *Case Stud. Constr. Mater.* 2024, 21:e03648.

[19] Huang X, Wang S, Lu T, Wu K, Li H, *et al*. Frost durability prediction of rubber concrete based on improved machine learning models, *Constr. Build. Mater.* 2024, 429:136201.

[20] Mi L, Mao J, Li L, Shi Q, Fang K, *et al*. Microstructural damage and durability of plateau concrete: Insights into freeze-thaw resistance and improvement strategies. *Structures* 2024, 60:105888.

[21] Han X, Ding N, Chen A, Wang Z, Xu Y, *et al*. Experimental study on freeze-thaw failure of concrete incorporating waste tire crumb rubber and analytical evaluation of frost resistance. *Constr. Build. Mater.* 2024, 439:137356.

[22] Li Z, Li L, Cheng S. Evaluation of modulus of elasticity of concrete containing both natural and recycled concrete aggregates. *J. Cleaner Prod.* 2024, 447:141591.

[23] Lundberg SM, Lee SI. A unified approach to interpreting model predictions. In *31st International Conference on Neural Information Processing Systems (NIPS)*, Long Beach, USA, December 4–9, 2017.

[24] Ribeiro MT, Singh S, Guestrin C. "Why should i trust you?": explaining the predictions of any classifier. In *Proceedings of the 22nd ACM SIGKDD International Conference on Knowledge Discovery and Data Mining*, New York, USA, August 13–17, 2016, pp. 1135–1144.

[25] Kolappan Geetha G, Sim SH. Fast identification of concrete cracks using 1D deep learning and explainable artificial intelligence-based analysis. *Autom. Constr.* 2022, 143:104572.

[26] Cui X, Lee M, Koo C, Hong T. Energy consumption prediction and household feature analysis for different residential building types using machine learning and SHAP: toward energy-efficient buildings. *Energy Build.* 2024, 309:113997.

[27] Elhishi S, Elashry AM, El-Metwally S. Unboxing machine learning models for concrete strength prediction using XAI. *Sci. Rep.* 2023, 13:19892.

[28] Jena R, Shanableh A, Al-Ruzouq R, Pradhan B, Gibril MBA, *et al*. Explainable artificial intelligence (XAI) model for earthquake spatial probability assessment in Arabian Peninsula. *Remote Sens.* 2023, 15:2248.

[29] Zhan J, Fang W, Love PED, Luo H. Explainable Artificial intelligence: counterfactual explanations for risk-based decision-making in construction. *IEEE Trans. Eng. Manage.* 2024, 71:10667–10685.

[30] Chakraborty D, Awolusi I, Gutierrez L. An explainable machine learning model to predict and elucidate the compressive behavior of high-performance concrete. *Results Eng.* 2021, 11:100245.

[31] Zhao W, Feng S, Liu J, Sun B. An explainable intelligent algorithm for the multiple performance prediction of cement-based grouting materials. *Constr. Build. Mater.* 2023, 366:130146.

[32] Zeng Z, Zhu Z, Yao W, Wang Z, Wang C, *et al*. Accurate prediction of concrete compressive strength based on explainable features using deep learning. *Constr. Build. Mater.* 2022, 329:127082.

[33] Cakiroglu C, Islam K, Bekdaş G, Isikdag U, Mangalathu S. Explainable machine learning models for predicting the axial compression capacity of concrete filled steel tubular columns. *Constr. Build. Mater.* 2022, 356:129227.

[34] Kulasooriya WKVJB, Ranasinghe RSS, Perera US, Thisovithan P, Ekanayake IU, *et al*. Modeling strength characteristics of basalt fiber reinforced concrete using multiple explainable machine learning with a graphical user interface. *Sci. Rep.* 2023, 13:13138.

[35] Aladsani M, Burton H, Abdullah S, Wallace J. Explainable machine learning model for predicting drift capacity of reinforced concrete walls. *ACI Struct. J.* 2022, 119:191–204.

[36] Ebrahimi K, Daiezadeh MJ, Zakertabrizi M, Zahmatkesh F, Habibnejad Korayem A. A review of the impact of micro- and nanoparticles on freeze-thaw durability of hardened concrete: mechanism perspective. *Constr. Build. Mater.* 2018, 186:1105–1113.

[37] Shang HS, Song YP. Experimental study of strength and deformation of plain concrete under biaxial compression after freezing and thawing cycles. *Cem. Concr. Res.* 2006, 36:1857–1864.

[38] Collins AR. The destruction of concrete by frost. *J. Inst. Civ. Eng.* 1944, 23:29–41.
[39] Penttala V, Al-Neshawy F. Stress and strain state of concrete during freezing and thawing cycles. *Cem. Concr. Res.* 2002, 32:1407–1420.
[40] Bai J, Zhao Y, Shi J, He X. Damage degradation model of aeolian sand concrete under freeze–thaw cycles based on macro-microscopic perspective. *Constr. Build. Mater.* 2022, 327:126885.
[41] Bumanis G, Dembovska L, Korjakins A, Bajare D. Applicability of freeze-thaw resistance testing methods for high strength concrete at extreme −52.5 °C and standard −18 °C testing conditions, *Case Stud. Constr. Mater.* 2018, 8:139–149.
[42] Guan X, Chen J, Qiu J, Gao Y, Gao J. Damage evaluation method based on ultrasound technique for gangue concrete under freezing-thawing cycles. *Constr. Build. Mater.* 2020, 246:118437.
[43] Panoutsopoulou L, Mouzakis C. Experimental investigation of the behavior of traditional timber mortise-tenon T-joints under monotonic and cyclic loading. *Constr. Build. Mater.* 2022, 348:128655.
[44] Bogas JA, de Brito J, Ramos D. Freeze–thaw resistance of concrete produced with fine recycled concrete aggregates. *J. Cleaner Prod.* 2016, 115:294–306.
[45] Çavdar A. Investigation of freeze–thaw effects on mechanical properties of fiber reinforced cement mortars. *Composites, Part B* 2014, 58:463–472.
[46] Grinys A, Augonis A, Daukšys M, Pupeikis D. Mechanical properties and durability of rubberized and SBR latex modified rubberized concrete. *Constr. Build. Mater.* 2020, 248:118584.
[47] Wen Y, Sun H, Hu S, Xu G, Wu X, *et al*. Microstructure and life prediction model of steel slag concrete under freezing-thawing environment. *Nanotechnol. Rev.* 2021, 10:1776–1788.
[48] Dong W, Shen X, Xue H, He J, Liu Y. Research on the freeze-thaw cyclic test and damage model of Aeolian sand lightweight aggregate concrete. *Constr. Build. Mater.* 2016, 123:792–799.
[49] Yang Z, Zhang A, Sudjianto A. GAMI-Net: an explainable neural network based on generalized additive models with structured interactions. *Pattern Recognit.* 2021, 120:108192.
[50] Nori H, Jenkins S, Koch P, Caruana R. InterpretML: a unified framework for machine learning interpretability. *arXiv* 2019, arXiv:1909.09223.
[51] Chen T, Guestrin C. XGBoost: a scalable tree boosting system. In *Proceedings of the 22nd ACM SIGKDD International Conference on Knowledge Discovery and Data Mining*, New York, USA, August 13–17, 2016, pp. 785–794.
[52] MAIF/shapash. 2023. Available: https://github.com/MAIF/shapash (accessed on 22 April 2023).
[53] Lee Y, Park J, Cho S. Extraction and prioritization of product attributes using an explainable neural network. *Pattern Anal. Appl.* 2020, 23:1767–1777.
[54] Murdoch WJ, Singh C, Kumbier K, Abbasi-Asl R, Yu B. Definitions, methods, and applications in interpretable machine learning. *Proc. Natl. Acad. Sci. U.S.A.* 2019, 116:22071–22080.
[55] Kruschel S, Hambauer N, Weinzierl S, Zilker S, Kraus M, *et al.* Challenging the performance-interpretability trade-off: an evaluation of interpretable machine learning models. *Bus. Inf. Syst. Eng.* 2025.
[56] Shah V, Jagupilla SCK, Vaccari DA, Gebler D. Non-linear visualization and importance ratio analysis of multivariate polynomial regression ecological models based on river hydromorphology and water quality. *Water* 2021, 13:2708.
[57] Hastie TJ. Generalized additive models. In *Statistical Models in S*. London: Routledge, 1992.
[58] Nanfack G, Temple P, Frênay B. Learning customised decision trees for domain-knowledge constraints. *Pattern Recognit.* 2023, 142:109610.
[59] Liu G, Sun B. Concrete compressive strength prediction using an explainable boosting machine model. *Case Stud. Constr. Mater.* 2023, 18:e01845.
[60] Feng DC, Wang WJ, Mangalathu S, Taciroglu E. Interpretable XGBoost-SHAP machine-learning model for shear strength prediction of Squat RC walls. *J. Struct. Eng.* 2021, 147(11):04021173.
[61] Liu D, Tu Y, Shi P, G Sas, Elfgren L. Mechanical and durability properties of concrete subjected to early-age freeze–thaw cycles. *Mater. Struct.* 2021, 54:211.
[62] An X, Che J, Liu H, Yang S, Doh SI. Study on freeze-thaw resistance with NaCl of desert sand engineering cement composites. Phys. Chem. Earth. A/B/C/ 2021, 121:102954.

[63] Yao L, Fang Z, Xiao Y, Hou J, Fu Z. An intelligent fault diagnosis method for lithium battery systems based on grid search support vector machine. *Energy* 2021, 214:118866.

[64] Sharma N, Malviya L, Jadhav A, Lalwani P. A hybrid deep neural net learning model for predicting coronary heart disease using randomized search cross-validation optimization. *Phys. Chem. Earth.* 2023, 9:100331.

[65] Dong S, Wu X, Qi X, Affolter C, Terrasi GP, *et al*. Prediction model of long-term tensile strength of glass fiber reinforced polymer bars exposed to alkaline solution based on Bayesian optimized artificial neural network. *Constr. Build. Mater.* 2023, 400:132885.

[66] Li W, Cai L, Wu Y, Liu Q, Yu H, *et al*. Assessing recycled pavement concrete mechanical properties under joint action of freezing and fatigue via RSM. *Construct. Build. Mater.* 2018, 164:1–11.

[67] Guo J, Guo T, Zhang S, Lu Y. Experimental study on freezing and thawing cycles of shrinkage-compensating concrete with double expansive agents. *Materials* 2020, 13:1850.

[68] Nicula LM, Corbu O, Iliescu M. Influence of blast furnace slag on the durability characteristic of road concrete such as freeze-thaw resistance. *Procedia Manuf.* 2020, 46:194–201.

[69] Baykal G, Saygılı A. A new technique to improve freeze–thaw durability of fly ash. *Fuel* 2012, 102:221–226.